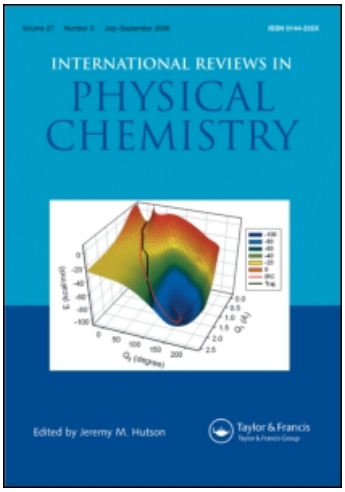

International Reviews in Physical Chemistry
Publication details, including instructions for authors and subscription information:
http://www.informaworld.com/smpp/title~content=t713724383

REMPI in a focusing rf-quadrupole: a new source for mass-, energy-, and state-selected ions

S. Mark[a]; Th. Glenewinkel-Meyer[a]; D. Gerlich[a]
[a] Institut für Physik, Technische Universität, Chemnitz, Germany

To cite this Article Mark, S. , Glenewinkel-Meyer, Th. and Gerlich, D.(1996) 'REMPI in a focusing rf-quadrupole: a new source for mass-, energy-, and state-selected ions', International Reviews in Physical Chemistry, 15: 1, 283 — 298
To link to this Article: DOI: 10.1080/01442359609353185
URL: http://dx.doi.org/10.1080/01442359609353185

INTERNATIONAL REVIEWS IN PHYSICAL CHEMISTRY, 1996, VOL. 15, NO. 1, 283–298

REMPI in a focusing rf-quadrupole: a new source for mass-, energy-, and state-selected ions

by S. MARK, TH. GLENEWINKEL-MEYER and D. GERLICH
Institut für Physik, Technische Universität, 09107 Chemnitz, Germany

Using resonance enhanced multiphoton ionization (REMPI), ions are created in a small volume centred on the axis of an rf-quadrupole. The pulsed beam of neutral molecular precursors is injected coaxially. This combination leads to high collection efficiency without the need of strong electrostatic extraction fields. The quadrupole is operated in the adiabatic limit. Therefore, the influence of the oscillatory rf-field on the ion trajectories can be described by an effective harmonic potential, which has focusing properties. Using these energy and mass dependent focusing properties, a primary H_2^+ beam of well-defined kinetic energy (< 5 meV (fwhm) at a mean of 50 meV) is prepared. In a typical case of multiphoton ionization of polyatomic molecules using C_2H_2, suppression of fragment ions by more than a factor of 10 is achieved, without losing the narrow kinetic energy spread of the parent ion beam.

1. Introduction

Photoionization has become a widely used technique for the preparation of state-selected ions in the study of ion molecule reactions in the gas phase and has already been reviewed extensively by Anderson (1992), Koyano and Tanaka (1992), and Ng (1992). Photoionization has historically been most applied to the investigation of the ionization process itself. For the production of primary ion species to study ion molecule reactions, especially at very low collision energies, the advantages of this method are relatively easy control over internal state and, to a lesser extent, over kinetic energy distributions. Both are very important factors in high resolution experiments to unravel the influence of vibrational or rotational energy. Vibrational spacings, for example, lie in the range of 100–400 meV, whilst low rotational states are spaced even closer, from about 15 meV for $J = 0$ to $J = 1$ in hydrogen, which would be the largest. Complete control over all three desired quantities, i.e. mass selectivity, kinetic energy spread, and internal state distribution has, however, not yet been achieved. A variety of ion sources has been described in the literature, which use single- or multiphoton ionization to produce a primary ion beam in well-defined internal states and show varied performance with respect to resolving energy and mass of the primary ion species.

In the pioneering work of Chupka *et al.* (1968) and Chupka and Russell (1968) primary ions have been created directly in the reaction cell by single photon ionization in the vacuum ultraviolet (VUV). In all further developments (e.g. Campbell *et al.* 1980) the ion source and the reaction region have been separated spatially in order to be able not only to distinguish safely between the ionization process and the reaction dynamics but also to achieve control over the collision energy and the distribution of internal states. These experiments include, among others, the threshold photoelectron photoion coincidence (TPEPICO), for example by Baer *et al.* (1979) and its improvement by Govers *et al.* (1984), and the threshold electron secondary ion coincidence method (TESICO) by Tanaka and Koyano (1978). In most sources,

0144-235X/96 $12·00

however, strong electrostatic extraction fields are used for ion collection (Liao *et al.* 1984, Morrison *et al.* 1985), up to several V cm^{-1}, which considerably disturb the ion kinetic energy distributions.

Another approach is the earlier versions of the present device, where ion creation by single photon VUV or resonance enhanced multiphoton ionization (REMPI) *inside* rf-guides has been used to achieve state selectivity combined with high collection efficiency without the need for strong extraction fields, for example by Anderson *et al.* (1981) and their later improvements by Orlando *et al.* (1989). In the earliest experiments a 12-pole–8-pole structure was used so that it had almost no mass selective properties. Also, in this set-up a supersonic expansion of the molecular precursor crossed the ionization region more or less *perpendicular* to the eventual flight path of the ions. This still required weak dc-extraction fields and therefore introduced an additional uncertainty to the ion kinetic energy on deflecting the ions from their initial trajectory. In general, the closer the apparatus design gets to avoiding acceleration of the ion, i.e. conserving the velocity distribution of the neutral precursor, the better the performance in view of creating narrow energy distributions of the ion beam. For an rf-guide this includes operation in the adiabatic limit, where, on average, the ion absorbs no energy from the rf-field. The creation or injection of ions has to occur in an almost field-free region, i.e. preferably on the axis of the rf-guide, as does the extraction from the rf-field and injection into the reaction or detection part of the apparatus. Even if a larger ionization volume or acceptance area is desired, operation under adiabatic conditions has to be assured. This means, for example, that the ion should traverse the boundary region of the rf-field with a small enough velocity or that the rf-field should be switched on slowly, i.e. over many rf-periods, after applying the ionization light pulse.

With the aim of achieving even more complete state selectivity, a different approach was developed by Mackenzie and Softley (1994), essentially an adaptation of the ZEKE–PES method invented by Müller-Dethlefs and Schlag (1990). Here the state selectivity arises from the controlled excitation of Rydberg states in the precursor molecule. These states are then field ionized and accelerated into the initial direction of the molecular beam without the use of any rf-guiding fields. First measurements for the reaction of H_2^+ ions in $N^+ = 1$ with the neutral H_2 precursor molecules down to collision energies of about 40 meV have been reported by Mackenzie and Softley (1994). It has also been demonstrated than in such a single beam experiment collision energies as low as 1 meV can be achieved (Gerlich and Rox 1989). Combining this method of ion preparation with a guided beam set-up allows the separation of the neutral ion precursor beam from the target beam and the study of ion molecule reactions at very low collision energies. The major advantage of the field ionization method is that, contrary to direct photoionization methods which rely on the propensity rules for the ionization process (Schweizer *et al.* 1990, Xie and Zare 1990), here one has direct control over the angular momentum states of the primary ion. The disadvantage is still the reliance on a pulsed extraction field which, again, introduces uncertainties into the ion kinetic energy distribution.

Unfortunately, most photoionization methods, such as VUV ionization, mass analysed threshold ionization (MATI), and REMPI, often lead to significant fragmentation of the state-selected parent ion, especially for larger polyatomic molecules. This raises the need for mass selection after ionization. As one example, in the later versions of the rf-guide ion sources, Chiu *et al.* (1992) included a quadrupole mass filter between the ion source and the reaction cell in order to provide a pure state-

selected $C_2H_2^+$ beam. They succeeded in suppressing fragment ions on the neighbour masses 24, 25 and 27 down to 1% of the parent ion. However, in the high mass resolution mode the rf-field of a quadrupole significantly perturbs the kinetic energy of the transmitted ions due to rf-heating along the path of the trajectory. In a recent study attempts were made by Smolanoff *et al.* (1995) to narrow these ion beam kinetic energy distributions by improving the mechanical tolerances of the quadrupole and ion injection system and careful matching of the quadrupole and injection operation conditions. It was found that the best results were achieved when the mass selector was run in a low pass energy mode. They observed an increase in the width of the kinetic energy distribution of 50 meV over the initial source distribution, whilst still retaining a mass resolution of greater than 100 and a transmission efficiency of better than 50%.

Our idea was to improve on the present rf-guide designs and combine the conventional multiphoton ionization method with the focusing properties of a quadrupole, driven in the adiabatic high frequency limit where the operation conditions are different from those of the conventional mass filter mode, and a collinear primary molecular beam from which the ions are created (Mark 1992).

In the following sections we first describe the set-up and operating conditions of this new source for mass-, energy- and state-selected ions. We give two examples of its performance by reporting on the quality of the kinetic energy distributions of an H_2^+ beam created in this source and the possibilities for fragment mass suppression in the case of a $C_2H_2^+$ ion beam. We conclude with an outlook on the prospects for using this new ion preparation technique in experiments on reactions with slow, state-selected ions.

2. Experimental

2.1. *Instrumental details*

The experiments with the new photoionization source are performed in the experimentally well-characterized universal Guided Ion Beam (GIB) apparatus described in detail by Gerlich (1992). Figure 1 shows a sketch of the photoionization source where the ions are created *inside* the linear rf-quadrupole.

The desired harmonic potential inside the quadrupole requires its four rods to have hyperbolical shape. In standard quadrupole mass filters this is often approximated by solid, cylindrical rods, in which case, the diameter of the rods themselves has to be 1·148 times that of the inscribed circle of the quadrupole (Dawson 1976). This conventional design has the disadvantage of placing a large metal surface area in the vicinity of the ion beam and the location of ion creation. Instead, we decided to approximate the desired hyperbolical shape of each rod by 15 wires of 1 mm diameter mounted on thin hyperbolic stainless steel holders (figure 1). A total of five of these holders are used for support, however, only one is fixed to the wires to permit easy expansion and contraction at differing temperatures so as to avoid deformation. This improved design has several advantages: the overall metal surface area is much smaller and so are the chances of hitting these surfaces with a laser or an electron beam intersecting the quadrupole perpendicularly. The open design also allows for efficient pumping of the neutral precursor gas in order to avoid collisional relaxation or subsequent ion molecule reactions of the state-selected ions. Therefore, problems such as rotational state changing collisions can be avoided, which plague experiments where ionization and reaction volume are not separated. The fairly large inscribed radius of the quadrupole ($r_0 = 2$ cm) leads to a comparably greater distance between the guided ions and the metal surfaces over conventional designs, reducing the

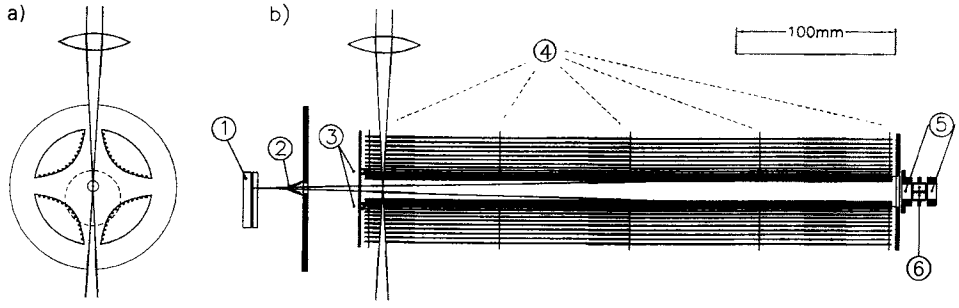

Figure 1. Quadrupole photoionization source. (*a*) shows a cross-sectional view along the quadrupole axis. Each of the hyperbolical mounting plates (0·5 mm thick) supports 15 thin wires which approximate a hyperbolic surface. The laser beam intersects the quadrupole perpendicularly. (*b*) shows a side view of the source: (1) piezo electric valve, (2) skimmer, (3) ion repeller plate, (4) hyperbolic mounting blocks, (5) and (6) einzel lens with deflection (pulsing) possibility.

influence of potential distortions on the ion motion. This seemingly complicated design allows easy matching and narrow tolerances because of the few non-standard (i.e. hyperbolic) surfaces, and is rather robust with respect to mechanical imperfections and defects since single wires and mounts can easily be replaced.

A pulsed piezoelectric nozzle injects the neutral precursor gas through a skimmer coaxially into the quadrupole. The nozzle skimmer distance is variable, but typically set to about 20 mm. With a nozzle diameter of 300 μm and a stagnation pressure of 2–4 bar a number density of about 10^{12} cm^{-3} is achieved at the location of ion creation, where the molecular beam has spread to a diameter of about 4 mm. The precursor gas pulses are about 50–70 μs long. The ionizing radiation (from a 30 Hz, 10 ns Quantel Nd:YAG pumped dye laser with doubling and mixing options) is focused onto the axis of the ion guide by a 10 cm lens. It intersects the quadrupole perpendicularly (figure 1) 61 mm downstream from the skimmer and the focus is roughly 300 μm in diameter.

H_2^+ ions were produced by 3+1 REMPI of neat H_2 used directly from the bottle (MG 5·0). Doubling the DCM output from the dye, laser pulse energies of 1–2 mJ have been achieved between 314 nm and 320 nm, with a resolution of 0·08 cm^{-1}. For $C_2H_2^+$ ion production 3+1 REMPI was used on 5% C_2H_2 (Air Liquide 2·6) seeded in high-purity helium (MG 5·0). The required wavelength (about 366 nm) for ionizing C_2H_2 via the $G^1\Pi_u$ state, obtained from mixing Rh6G dye laser output with the Nd:YAG fundamental output produced about 8 mJ per pulse with a resolution of ~ 1 cm^{-1}.

The number of ions created per laser shot was only about 20–30 in order to minimize distortions from space–charge effects. For this, the power density of the laser light was varied between 10^7 W cm^{-2} and 10^9 W cm^{-2}. In fact, space–charge effects were observed during these experiments, which considerably broaden the energy distributions as detected by the time-of-flight method. From the Poisson equation $\Delta\Phi = 4\pi\rho$ one can estimate that an ion density of 10^6 cm^{-3} would lead to an observable additional spread of the energy distributions of the order of a few meV. Since the laser focus volume is of the order of 10^{-6} cm^3 a few created ions already influence the measured distributions. Our experiments show that under these conditions and with 30 ions/laser shot the Coulomb repulsion leads to an additional widening of the centre-of-mass energy distribution by about 1·5 meV. Due to the initial centre-of-mass motion of the neutral precursor molecules this equates to almost 20 meV in the

laboratory reference frame, as calculated from vector addition of the contributing velocities.

The use of a molecular beam has the advantage of cooling the neutral gas during the adiabatic expansion from the nozzle, providing a narrow kinetic energy distribution. It also lowers the rotational temperature, which is favourable for the preparation of low rotational states. For the preparation of higher rotational states the pulsed valve is replaced by a simple effusive gas inlet consisting of a 1 mm diameter tube with its end very close ($\sim$ 3 mm) to the laser focus. In addition, the precursor molecules are already moving on-axis into the desired direction (figure 1), eliminating the need for strong electrostatic extraction fields which would affect the ion kinetic energy distribution. In previous designs, the molecular beam was positioned either perpendicularly to both the laser beam and the ion flight axis (Govers *et al.* 1984, Achtenhagen 1989) or under a 60° angle with respect to this axis (Anderson *et al.* 1981). Recent experiments by Schweizer *et al.* (1994) and Chiu *et al.* (1995) have already demonstrated the versatility and pre-eminence of the set-up described in this publication.

2.2. *Quadrupole, theory of operation*

A complete theoretical description of the quadrupole mass spectrometer or ion guide is given by Dawson (1976). The differential equation describing the trajectories of charged particles in $2n$-poles reduces to the well-known Mathieu differential equation in the special case of a quadrupole ($n = 2$). The region of stable operation is given by parameters a_2 and q_2 which are functions of the potential $V_0 \pm U_0$ applied to the two pairs of electrodes, from the rf-amplitude V_0 and the dc potential offset U_0, the rf-frequency $\Omega = 2\pi f$, the inscribed circle of the quadrupole r_0, and the mass m and charge q of the ions:

$$a_2 = \frac{8\,q\,U_0}{m\,\Omega^2\,r_0^2} \quad q_2 = \frac{4\,q\,V_0}{m\,\Omega^2\,r_0^2}. \tag{1}$$

To simplify the understanding of the specific transmission features of the quadrupole we are interested in, we make use of the effective potential (or adiabatic) approximation. An empirical relation, $q_2 < 0{\cdot}3$ (e.g. Gerlich 1992), gives a conservative estimate of an upper bound for the validity of the adiabatic limit. Within this approximation the derivation of conditions for operating a quadrupole in the focusing mode (Gerlich 1992) is straightforward: since the effective potential resulting from the rf-field with frequency $f = \Omega/2\pi$ is harmonic, the equations of motion can be separated into two harmonic oscillator differential equations, describing the x- and the y-components of the smooth motion independently. Both oscillate with different secular frequencies $\omega_{x,y}$:

$$\omega_{x,y} = \tfrac{1}{2}\beta_{x,y}\,\Omega \tag{2}$$

where

$$\beta_{x,y} = \left(\frac{q_2^2}{2} \pm a_2\right)^{1/2}. \tag{3}$$

The convention here is that the pair of electrodes defining the x-direction are on positive bias 2 U_0 with respect to the other pair. Without any dc voltage applied, i.e. for $U_0 = 0$ V, a_2 vanishes, the two frequencies $\omega_{x,y}$ are identical and the value of β is simply a multiple of q_2:

$$\beta_{x,y} = \frac{1}{\sqrt{2}}\,q_2. \tag{4}$$

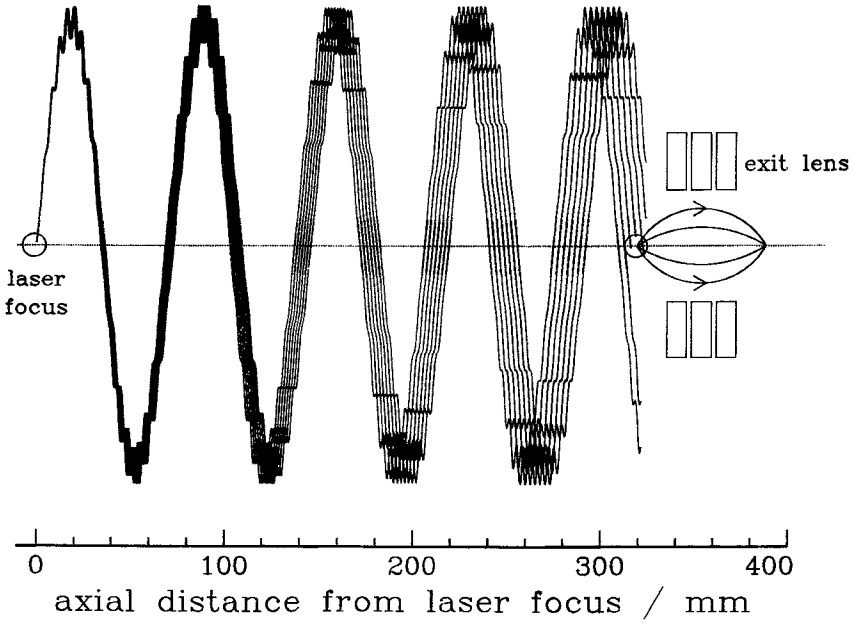

Figure 2. Illustration of the focusing properties of a quadrupole governed by equations (1)–(5). An initial packet consisting of ions (here, mass: 4 amu) with different kinetic energies (140–158 meV, 3 meV steps) is focused onto the exit aperture. These differences result in trajectories with distinct nodal patterns, giving rise to the peak structure in the observed time-of-flight spectra after spatial selection in the exit region.

With a superimposed dc potential difference U_0, i.e. $a_2 \neq 0$, the oscillation in the x-direction becomes faster than that in the y-direction.

Figure 2 depicts ion trajectories calculated for one particular set of (q_2, a_2) in which ω_x is the same as ω_y. If these two frequencies are different the flight time $t = s/v$, where v is the ion velocity, has to obey the two equations (N_x, N_y integer)

$$t = \frac{N_x \pi}{\omega_x} \quad \text{and} \quad t = \frac{N_y \pi}{\omega_y} \tag{5}$$

to image the ion ensemble from the central entrance aperture (i.e. the laser focus) onto the exit. Note that the exit aperture does not necessarily have to be defined by mechanical boundaries, and in our case it is the acceptance volume of a lens system which is mounted between the quadrupole and the octupole system of the GIB apparatus. In the simulation for figure 2 the kinetic energy of the individual trajectories was varied from 140 to 158 meV in steps of 3 meV. For the same set of (q_2, a_2) some ions with slightly different velocities are discriminated as shown because their flight time does not fulfil the equations (5) and they miss the acceptance volume of the exit lens. This effect is used for energy and also mass selection.

As already mentioned in the Introduction, the standard Paul filter mode ($q_2 = 0{\cdot}706$, $a_2 = 0{\cdot}237$) cannot be used for mass selection since these operating conditions are far outside of the adiabatic regime. However, inspection of the (a_2, q_2) stability diagram of the Mathieu differential equation reveals that one can make use of the low-mass band pass filter properties of the quadrupole. Since stable ion trajectories in the quadrupole field need to obey the relation

$$a_2 < \tfrac{1}{2} q_2^2 \tag{6}$$

only masses smaller than a critical value m_{crit}

$$m_{crit} = \frac{qV_0^2}{\Omega^2 r_0^2 U_0} \tag{7}$$

are transmitted and higher masses are efficiently discriminated against.

In the present experiment the mass dependence of the focusing properties (5) provided sufficient mass selection. The combination with the low-pass mode did not result in a significant improvement. In the following section we demonstrate that these features result in an H_2^+ beam with a very narrow axial kinetic energy distribution. In the case of ionizing C_2H_2 it is possible to discriminate against and suppress most of the fragment ions in the beam.

3. Results

3.1. *Energy selection*

To test the achievable energy resolution of the quadrupole photoinization source H_2^+ ions are produced by 3 + 1 REMPI using the R(1) transition from the ground state via $B^1\Sigma_u^+$ ($v' = 4$) at 315 nm. In a region around this wavelength Schweizer *et al.* (1990) demonstrated the possibility of systematic variation of the rotational energy content of the ions, relying on propensity rules for the ionization process. With a laser energy of 1·5 mJ per pulse, and a power density of 4×10^9 W cm^{-2} at the focus, approximately 50 ions per pulse have been created. The width of the ion kinetic energy distribution is determined by the velocity distribution of the molecular beam of the neutral precursor, the electrostatic potential gradient in the ionizing volume, and the Coulomb repulsion between the ions created in the photoionization event. Whereas the two former are under direct control of the experimentalist by choosing the expansion conditions of the supersonic molecular beam and the quality and design of the ion optics, respectively, the latter can only be avoided by judicious choice of the laser pulse power and focusing conditions. Increasing the laser power density beyond a certain limiting value will only create more ion intensity by broadening the kinetic energy distribution, rather than increasing the peak intensity of ions in a narrow range of energies.

Figure 3 shows three time-of-flight spectra illustrating the velocity-dependent focusing properties of the quadrupole. The top axis gives a scale of the corresponding kinetic energy of the ions. The dotted curves represent the axial kinetic energy distribution of the total ion ensemble produced at the laser focus, which is of course the same in all cases, having a width of 33 meV at this power density. The full curves are used for the resulting energy distribution after passage through the quadrupole. In all three cases the ion guide was operated with no dc bias, i.e. $U_0 = 0$ V, so that the ion trajectories undergo the same number of oscillations in the x- as well as in the y-direction. In the upper panel (*a*) the rf-voltage was set to $V_0 = 70$ V, which results in the trajectories of the ions being confined in a narrow region around the quadrupole axis. Therefore only a few ions are eliminated from the whole ensemble ($\sim 20\%$, the difference in area under the dotted and the full curves, respectively). The observed peak structure is a direct result of the nodal character in the ion trajectories and the transmission maxima can be assigned to node numbers $N_x = N_y = (20, \ldots, 24)$. In the middle panel (*b*), the rf-voltage has been reduced to $V_0 = 45$ V. The guiding field is still strong enough to confine most of the ions, but a larger fraction is suppressed. Their trajectories are characterized by larger amplitudes, and because of the smaller characteristic frequency ω, and smaller q_z value, the number of nodes decreases (here

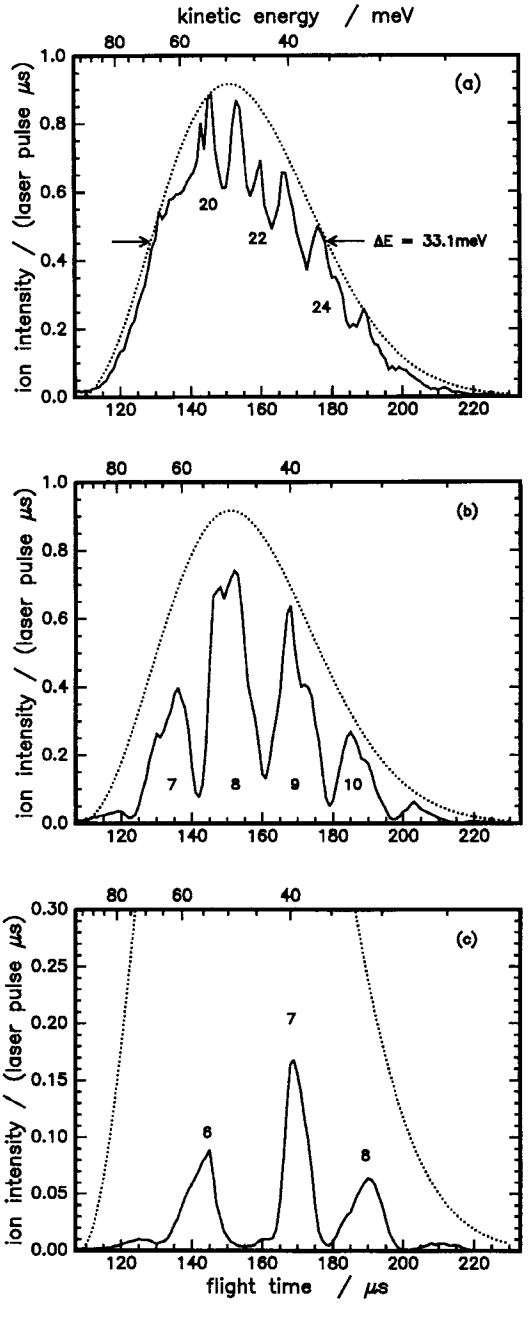

Figure 3. Time-of-flight distributions of the ion ensemble resulting from the focusing properties of the quadrupole. The initially created distribution is marked by a dotted curve. An rf-amplitude of $V_0 = 70$ V, top panel (*a*), creates a strong guiding field and leads to a high value of the characteristic angular frequency ω. This eliminates only few ions since the major fraction is confined on trajectories near the quadrupole axis and focused onto the exit aperture. It also produces a larger number of transmission maxima according to (5). At $V_0 = 45$ V, middle panel (*b*), and at $V_0 = 30$ V, bottom panel (*c*), both the guiding field strength and ω_x decrease. The amplitudes of the ion trajectories increase and the peak structure in the time-of-flight spectra becomes more pronounced.

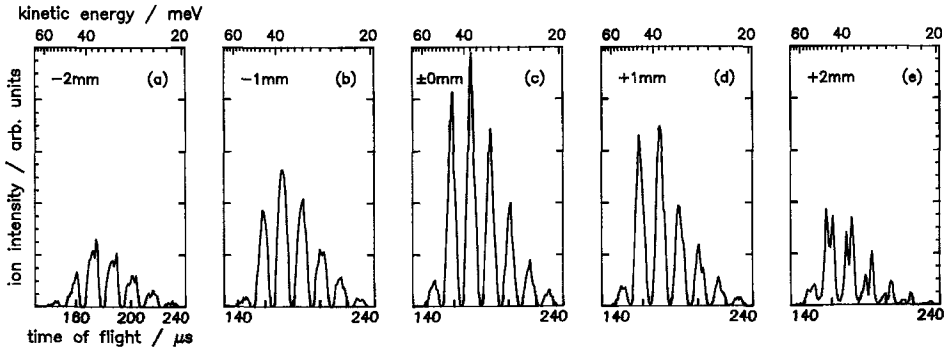

Figure 4. Dependence of the transmission properties of the quadrupole on the geometrical location of the laser focus. The operating conditions are the same as for figure 5, but the laser focus is moved 1 and 2 mm off-axis in both directions. The overall intensity decreases and substructures appear indicating differences in kinetic energy of less than 1 meV.

$N_x = N_y = 7, \ldots, 10$). The energy selection properties are far better then because fewer ions fulfil the imaging conditions (5). The lowest panel (*c*) shows the transmitted ion intensity for $V_0 = 30$ V. The maxima are even further apart and the number of nodes in the ion trajectories is now $N_x = N_y = 6, 7, 8$. It becomes obvious that better peak separation is achieved at the expense of overall ion intensity.

It should be noted, however, that the kinetic energy of the individual ions is not affected as the quadrupole is operated within the adiabatic approximation. It was shown (Gerlich 1992) that after a large number of rf-cycles, typically about 10^6, the average energy per ion absorbed from the rf-field is negligibly small under these operating conditions. Intervals of kinetic energy are filtered out by the exit aperture and a peak structure is left in the energy distribution (and in flight time), where every peak represents an individual subset of the complete ion ensemble with a remarkably narrow energy spread. With the aid of a split electrode, which is part of the exit lens system ((6) in figure 1), appropriate pulsing of its bias voltage allows the selection of single transmission maxima as they are 'passing by' and results in a very narrow final ion energy distribution. Since the transmission minima are rather wide, precise setting of the pulse rise and fall-off avoids acceleration or deceleration of the transmitted ions and allows complete separation of the individual peaks.

For highest energy selection a number of parameters has to be optimized: the mechanical quality of the quadrupole, stability of the rf-guiding field, but also the focusing properties of the laser and the details of the molecular and laser beam geometry. In figure 4 the influence of the location of the laser focus, and therefore of the created ion cloud, with respect to the centre of the quadrupole is investigated. The series of panels in this figure corresponds to moving the laser focus perpendicularly across the quadrupole axis in steps of 1 mm. The centre panel marks the optimum position. Off-axis deviation of only 1 mm clearly leads to a drastic decrease in ion intensity on the one hand. Since the pulsed nozzle is located at a distance of 8·1 cm upstream from the laser focus the molecular beam diameter is already greater than 4 mm in the ionization region. Therefore, this decrease is not due to a drop in the number density of the precursor gas, but rather it is caused by the transmission properties of the quadrupole. Another 1 mm shift diminishes the ion signal even further, but also causes interesting substructures in the time-of-flight peaks. They may

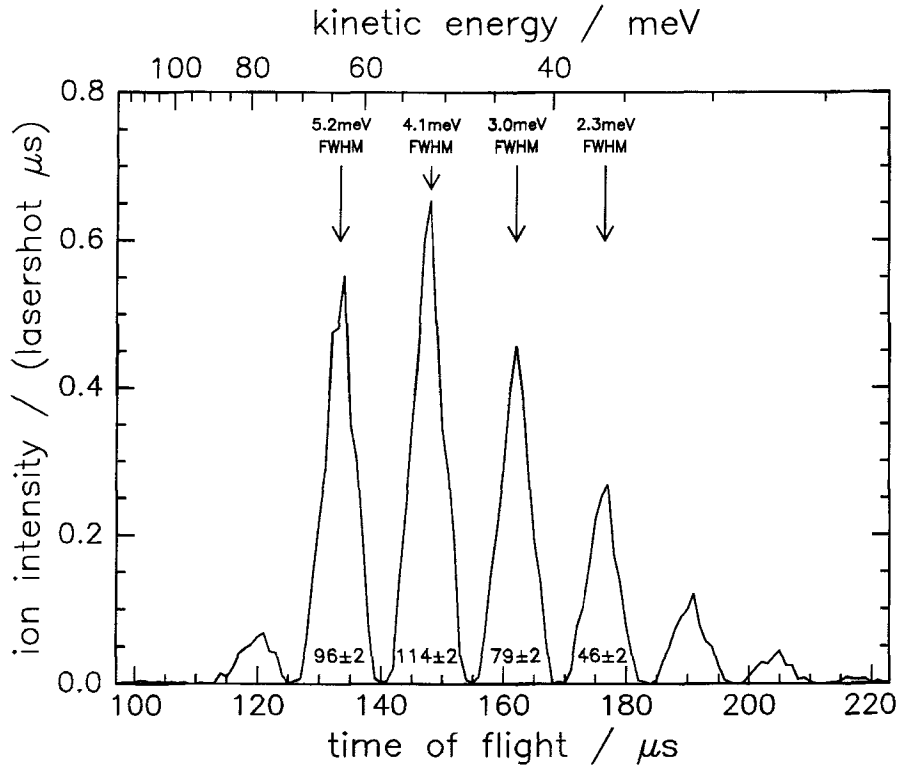

Figure 5. Time-of-flight spectrum of H_2^+ ions obtained with optimized quadrupole operating parameters $V_0 = 60$ V, $U_0 = 0$ V, $f = 7{\cdot}2$ MHz. The principal peak represents an ion ensemble with an average kinetic energy of ~ 50 meV and a half width of 4·1 meV (fwhm). Its intensity is 110 ions s^{-1}. The number of nodes in the trajectories of the ions that contribute to this peak is $N_x = N_y = 10$.

correspond to variations/differences in kinetic energy in the sub-meV range but might also be due to rf-phase dependent influences: the duration of the laser pulse is short compared to the rf-period. Since laser and the phase of the rf-field are not synchronized, in the off-axis region ions are now created in a regime where the rf-field affects their initial kinetic energy. Therefore, the substructure could be caused by time-focusing of ions with phase dependent initial kinetic energies.

Figure 5 reproduces the middle panel of figure 4, the result of the optimum operating conditions. The quadrupole parameters in this case are $V_0 = 60$ V, $U_0 = 0$ V, $f = \Omega/2\pi = 7{\cdot}2$ MHz, so that a particle of mass 2 amu experiences an effective potential of 212 meV at $r/r_0 = 1$. Note also the extremely small value of the stability parameter $q_z = 0{\cdot}014$. The principal peak at a flight time of 148 μs represents an ion ensemble with an average laboratory kinetic energy of 50 meV and a spread of only 4·1 meV (fwhm). Its intensity of 114 ions s^{-1} is sufficient for measurements of reliable absolute integral cross-sections in the Guided Ion Beam apparatus. However, the width of the individual peaks in energy space becomes narrower on moving to longer flight times. Sacrificing for ion intensity it is possible to select a different feature with less energy spread in the time-of-flight spectrum, such as the peak around 175 μs in figure 5, where the full-width-half-maximum decreased to only 2·3 meV and the average kinetic energy of an ion in the quadrupole is a mere 35 meV. By acceleration

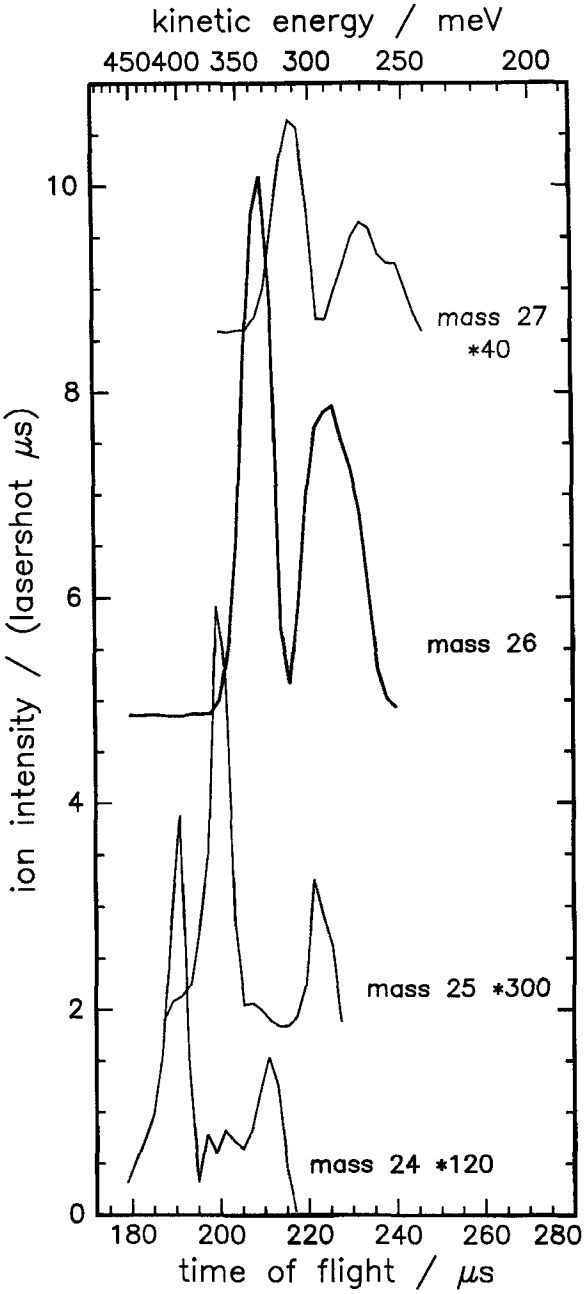

Figure 6. Mass dependence of the focusing properties for acetylene photoionized by 3+1 REMPI. Time-of-flight distributions for ions with masses 24, 25, 26 and 27 are shown. The transmission maxima, for $N_x = 10$, are clearly separated.

of these ions into the octupole a beam with very well-defined laboratory kinetic energy can be prepared, and deceleration to a few meV is also possible.

3.2. *Mass selection*

$C_2H_2^+$ has become a prototypical primary ion for small polyatomic systems (Hawley and Smith 1989, Adams and Smith 1977, Orlando *et al.* 1989, 1990, Chiu *et al.* 1994, 1995). Several of its reactions are very sensitive to the internal energy content of the $C_2H_2^+$ ion. REMPI has so far been the method of choice to prepare a state-selected $C_2H_2^+$ beam. It turns out, though, that multiphoton ionization always leads to a considerable amount of fragment ions, C_2H^+ and even C_2^+. In most cases, C_2H^+ is much more reactive, so that even small impurities may lead to quite large uncertainties when unravelling the contributions of separate species to the reaction under investigation. In addition, the acetylene ion isotope $^{13}C^{12}CH_2^+$ (with a natural abundance of $\sim 2\%$) masks the production of $C_2H_3^+$ in some important reactions. We used the mass selective focusing properties of our rf-quadrupole source to get closer to the goal of preparing a pure state-selected $C_2H_2^+$ beam with a well-defined kinetic energy distribution.

The rf-frequency was lowered to $f = 3{\cdot}5$ MHz, compared to the hydrogen experiment, and the ion beam and the focusing properties of the quadrupole were optimized for mass 26, the acetylene ion, to give $V_0 = 231$ V, $U_0 = 18$ mV. The time-of-flight spectra for the masses 24, 25, 26 and 27 in figure 6 show similar transmission maxima and minima; according to (5) the main maxima have to be attributed to $N_x = 10$ (marked as N_{10}); their mass dependence is of course obvious. We repeated the measurements for much higher laser power and larger ion intensities in order to characterize a primary beam with high count rates. The operating conditions were again adjusted for optimal transmission of mass 26 and maximum rejection of the unwanted contributions and resulted in the parameter set $V_0 = 204$ V, $U_0 = 7$ mV. These time-of-flight spectra are depicted in figure 7, similar to the previous figure, but now with a logarithmic intensity scale. The different symbols mark the experimental points whereas the lines result from a spline fit and are only used to guide the eye of the reader. The dashed vertical lines at a flight time of about 240 μs indicate the temporal location of the 10 μs pulser gate to allow passage of only a narrow ion packet.

The resulting packet is characterized in figure 8(*a*). The ensemble has an average kinetic energy of 250 meV with a half width of ~ 17 meV (remember the logarithmic scale). The ion intensity is about 560 ions s^{-1}. The relative intensities of the different ion masses determined from the peak areas are depicted in a bar graph in figure 8(*b*) (again using a logarithmic intensity scale). The dotted bars represent the original mass ratios after creation of the ion packet at the laser focus and reproduce well earlier results of Orlando *et al.* (1989), and the solid bars represent the improved mass ratios on exit from the quadrupole running under optimized conditions. This allows discrimination against $\sim 90\%$ of both fragment ions (mass 24 and 25), and simultaneously $> 80\%$ of mass 27 could be suppressed. The final intensity ratio between the desired mass 26 and the minor contributions at 24, 25 and 27 was then less than 0·2 % in all three cases, and for the especially important C_2H^+ ion, mass 25, it was even less than 0·09 %.

We have also tried to reduce the contributions from unwanted higher masses by making use of the low-pass filter properties, see §2, equation (7). Discrimination of mass 27 has indeed been improved, but at the expense of discrimination against the

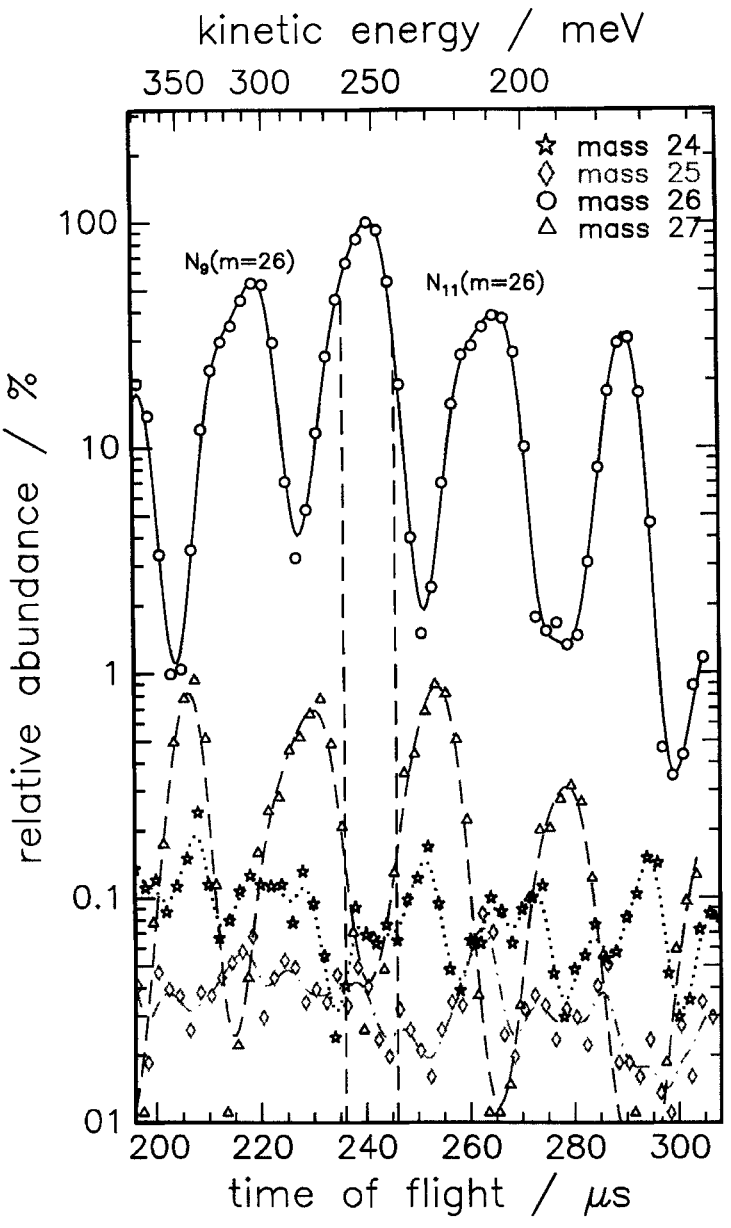

Figure 7. Time-of-flight spectra for masses 24, 25, 26 and 27, on a logarithmic intensity scale, for optimized parameters for the acetylene ion ($V_0 = 204$ V, $U_0 = 7$ mV, $f = 3{\cdot}5$ MHz). The discrimination of unwanted contributions is most pronounced for a flight time at around 240 μs, where we also pulse the gate of the split exit lens, as indicated by the vertical dashed lines.

fragment ions. For this mode of operation the parameters have been independently optimized, and about the same degree of mass selectivity of the $C_2H_2^+$ beam has been achieved, though the total ion intensities were somewhat lower.

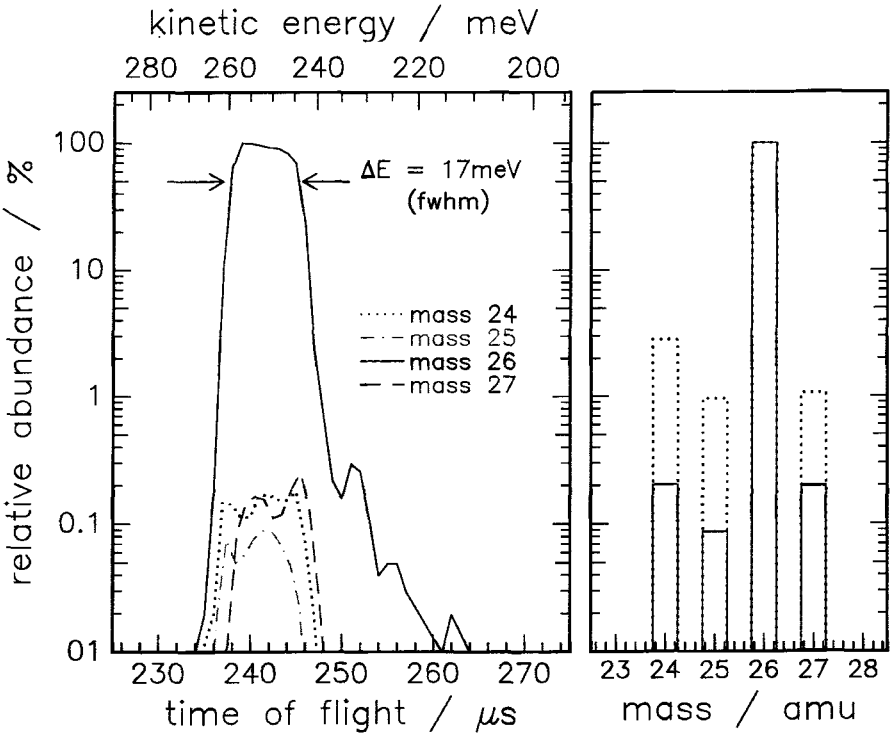

Figure 8. Time-of-flight spectra of the acetylene ion beam resulting from gating of the exit aperture. The timing of the gate pulse with respect to the time-of-flight peaks is indicated in the previous figure. The ion intensities are depicted on a logarithmic scale in both panels. The kinetic energy spread is about 17 meV (fwhm) at a mean laboratory energy of ~ 250 meV. On the left, the raw spectra are shown, on the right a bar graph of the integrated peak intensities is displayed, comparing the abundance of neighbouring masses in the original ion packet and data from Orlando *et al.* (1989) (dotted) with the final optimized result of the present set-up (solid). 90 % of the ions of the lower masses 24 and 25 and $\frac{2}{3}$ of the ions of mass 27 have been eliminated. The total ion intensity at mass 26 is 550 ions s^{-1}.

4. Summary

We have presented a new version of a mass-, energy- and state-selective ion source. On-axis photoionization inside an rf-quadrupole provides high ion collection efficiency, a well-defined ionization volume, and phase space conserving imaging properties. Combined with coaxial injection of the neutral molecular precursor beam, which avoids the need for electrostatic potential gradients and their associated problems, this lowers the attainable minimum collision energy and the width of its associated distribution significantly. The open design of the quadrupole rods allows for efficient pumping of the neutral precursor gas; therefore collisional relaxation and subsequent ion molecule reactions of state-selected ions are avoided. The large inscribed radius of the quadrupole minimizes the fringe effects from potential distortions on the metal surfaces, resulting in nearly perfect transmission properties at meV energies.

Characterization of the transmission properties revealed that under typical operation conditions an H_2^+ ion packet with a mean laboratory kinetic energy of 50 meV and a width of 4 meV (fwhm) is easily achieved. Sacrificing for intensity, these

extremely good values could be improved to a mean of 35 meV with a width of a mere 2·3 meV. A $C_2H_2^+$ beam was prepared with an energy spread of $\sim$ 17 meV at 250 meV mean laboratory energy and an intensity of $\sim$ 560 ions s^{-1}. 90% of the naturally-occurring fragment ions and isotopes were suppressed, so that less than 0·2% of each impurity remained in the primary beam.

These mass and energy selection properties were achieved by taking advantage of the focusing properties of the quadrupole field within the adiabatic limit.

5. Outlook

Naturally, the new set-up presented allows several modifications and a variety of different enhancements.

Additional suppression of minority species in the ion beam could be achieved by applying auxiliary rf-fields along the quadrupole. These field frequencies need to match the resonance frequency $\omega_{x,y}$ given by (2). This would selectively heat the chosen impurity by resonant excitation and result in divergent trajectories eliminating these ions. Studies to this end were performed by Watson *et al.* (1989) and Eckart (1990).

Other experiments could include merging the primary ion beam with a reaction partner from another pulsed, supersonic expansion, or letting the ions react with the seed gas or neutral precursor inside the quadrupole. Similar studies were done by Mackenzie and Softley (1994) on bimolecular reactions of H_2^+ ions with H_2, already mentioned above, and by Gerlich and Rox (1989) on the three-body association reaction of CO^+ with CO to produce $(CO)_2^+$.

Those same experiments by Mackenzie and Softley (1994) made use of generating Rydberg states and produced the ions with subsequent pulsed field ionization. This method could be a logical enhancement of the presented set-up and could be combined with detection of the photoelectrons by a microchannel plate in the backward direction of the ion beam. The pulsed expansion of neutral Rydberg states would pass through a hole in the channel plate and be ionized directly in front of the plate. This would enable the use of a scheme similar to TESICO by Tanaka and Koyano (1978) to further aid the characterization of the ion state distribution. In order to overcome the difficulties with perturbations in the kinetic energy distributions arising from the pulsed ionization field, the electron would be removed by a delayed infrared laser pulse inside a small homogeneous dc electric field. The total electron intensity then also provides for easy shot-to-shot calibration of the number of primary ions.

Other experiments could include the possibility of subsequently vibrationally exciting the molecular ions at an intermediate focus or at the quadrupole exit aperture. This would allow the study of reactions of ions with large amounts of well-defined excitation, say 2 or 3 quanta of C–H stretching vibration in a larger hydrocarbon ion or similar primary reaction partners.

Finally, the almost perfect focusing phase space conserving properties of the quadrupole would allow the investigation of the ionization process itself by imaging the photoions and photoelectrons on microchannel plates on opposite sides of the ionization region. Xie and Zare (1990) and Wiedmann *et al.* (1993) were pioneering some of this experimental work and, especially, Xie and Zare (1990) elucidated the theoretical background on simple systems. The properties to study would be vector correlations between polarization of the incident radiation and velocity and angular momentum distributions through time-of-flight spectroscopy in the quadrupole.

The promising versatility of the presented set-up will hopefully contribute to

unravelling important questions in the field of low collision energy ion molecule reactions.

Acknowledgments

Financial support of the Deutsche Forschungsgemeinschaft (Sonderforschungsbereich 276, Freiburg, and Innovationskolleg 2, Chemnitz) and the European Community (Human Capital and Mobility programme) is gratefully acknowledged.

References

ACHTENHAGEN, M., 1989, Diplom thesis, Universität Freiburg, Germany.
ADAMS, N. G., and SMITH, D., 1977, *Chem. Phys. Lett.* **47,** 383.
ANDERSON, S. L., 1992, *Adv. chem. Phys.*, **LXXXII,** 177.
ANDERSON, S. L., HOULE, F. A., GERLICH, D., and LEE, Y. T., 1981, *J. chem. Phys.*, **75,** 2153.
BAER, TH., GUYON, P. M., NENNER, I., TABCHÉ-FOUHAILLÉ, A., BOTTER, R., FERREIRA, L. F. A., and GOVERS, T. A., 1979, *J. chem. Phys.*, **70,** 1585.
CAMPBELL, F. M., BROWNING, R., and LATIMER, C. J., 1980, *J. Phys. B.*, **14,** 1183.
CHIU, Y., FU, H., HUANG, J., and ANDERSON, S. L., 1994, *J. chem. Phys.*, **101,** 5410.
CHIU, Y., FU, H., HUANG, J., and ANDERSON, S. L., 1995, *J. chem. Phys.*, **102,** 1199.
CHIU, Y., YANG, B., FU, H., ANDERSON, S. L., SCHWEIZER, M., GERLICH, D., 1992, *J. chem. Phys.*, **96,** 5781.
CHUPKA, W. A., and RUSSELL, M. E., 1968, *J. chem. Phys.*, **48,** 1527; *ibid.*, **49,** 5426.
CHUPKA, W. A., RUSSELL, M. E., and REFAEY, K., 1968. *J. chem. Phys.*, **48,** 1518.
DAWSON, P. H., 1976, *Quadrupole Mass Spectrometry* (Amsterdam: Elsevier Scientific Publishing).
ECKART, C., 1990, Diplom thesis, Universität Freiburg, Germany.
GERLICH, D., 1992, *Adv. chem. Phys.*, **LXXXII,** 1.
GERLICH, D., and ROX, T., 1989, *Z. Phys.* D, **13,** 259.
GOVERS, R., GUYON, P. M., BAER, TH., COLE, K., FRÖHLICH, H., and LAVOLLÉE, M., 1984, *Chem. Phys.*, **87,** 373.
HAWLEY, M., and SMITH, M. A., 1989, *J. Am. chem. Soc.*, **111,** 8293.
KOYANO, I., and TANAKA, K., 1992, *Adv. chem. Phys.*, **LXXXII,** 263.
LIAO, C. L., LIAO, C. X., and NG, C. Y., 1984, *J. chem. Phys.*, **81,** 5672; 1985, *ibid.*, **82,** 5489.
MACKENZIE, S. R., and SOFTLEY, T. P., 1994, *J. chem. Phys.*, **101,** 10609.
MARK, S., 1992, Diplom thesis, Universität Freiburg, Germany.
MORRISON, R. J. S., CONAWAY, W. E., and ZARE, R. N., 1985, *Chem. Phys. Lett.* **113,** 435.
MÜLLER-DETHLEFS, K., and SCHLAG, E., 1990, *Ann. Rev. phys. Chem.*, **42,** 109.
NG, C. Y., 1992, *Adv. chem. Phys.*, **LXXXII,** 401.
ORLANDO, T. M., YANG, B., and ANDERSON, S. L., 1989, *J. chem. Phys.*, **90,** 1577.
ORLANDO, T. M., YANG, B., CHIU, Y., and ANDERSON, S. L., 1990, *J. chem. Phys.*, **92,** 7356.
SCHWEIZER, M., JERKE, G., and GERLICH, D., 1990, *MOLEC VIII Book of Abstracts* (Universität Kaiserslautern: Germany), p. 175.
SCHWEIZER, M., MARK, S., and GERLICH, D., 1994, *Int. J. Mass. Spectr. Ion Processes*, **135,** 1.
SMOLANOFF, J., LAPICKI, A., and ANDERSON, S. L., 1995, *Rev. Sci. Instrum.*, **66**, 3706.
TANAKA, K., and KOYANO, I., 1978, *J. chem. Phys.*, **69,** 3422.
WATSON, J. T., JAOUEN, D., MESTDAGH, H., and ROLANDO, C., 1989, *Int. J. Mass Spectr. Ion Processes*, **93,** 225.
WIEDMANN, R. T., WHITE, M. G., WANG, K., and MCKOY, V., 1993, *J. chem. Phys.*, **98,** 7673.
XIE, J., and ZARE, R. N., 1990, *J. chem. Phys.*, **93,** 3033; 1992, *ibid.*, **97,** 2891.